Accurate response of wing structures to free-vibration, load factors and non-structural masses

Accurate response of wing structures to free vibration, load factors and non-structural masses

Erasmo Carrera[1] and Alfonso Pagani[2]
Department of Mechanical and Aerospace Engineering,

Politecnico di Torino, Corso Duca degli Abruzzi 24, 10129 Torino, Italy

Based on the Carrera Unified Formulation (CUF), this work extends variable kinematic finite beam elements to include load factors and non-structural masses for the static and vibration analyses of complex, metallic wing structures. According to CUF, variable kinematic beam theories are formulated in an automatic and hierarchical manner by expressing the displacement field as an arbitrary expansion through generic cross-sectional functions. Both Taylor-like and Lagrange polynomials are used in this paper to develop refined beam kinematics, and the related theories are referred to as TE and LE, respectively. The generalized unknowns of TE models are the beam axis displacements and the N-order displacement derivatives, N being a free parameter of the analysis. Classical beam theories are clearly particular cases of the linear ($N = 1$) TE model. On the other hand, LE models have only pure translational displacements as unknowns. By exploiting this characteristic of LE, a Component-Wise (CW) approach is implemented and used for the analysis of multi-component reinforced-shell structures. Numerical applications are developed by classical finite element procedures, and both static response and free vibration analyses are addressed. Various configurations of a benchmark wing are considered, and the capabilities of the present methodologies when dealing with higher-order effects due to deformable cross-sections and geometrical discontinuities (e.g. underside windows) are evaluated. The attention is focused on the applicability of the present refined beam models to problems

---

[1] Professor of Aerospace Structures and Aeroelasticity, and AIAA Member. E-mail: erasmo.carrera@polito.it
[2] Research Fellow. E-mail: alfonso.pagani@polito.it

involving complex, external inertial loadings. The results are compared to finite element solutions from commercial tools, including full 3D models and models obtained by assembling 2D shell and 1D finite elements.

Nomenclature

E	Elastic modulus
F_τ	cross-section functions
G	shear modulus
$\mathbf{K}^{ij\tau s}$	fundamental nucleus of the elemental stiffness matrix
l	dimension of the structure in the y direction
L_{ext}	work of external loadings
L_{ine}	work of inertial loadings
L_{int}	strain energy
M	number of expansion terms
$\tilde{m}$	non-structural mass
$\mathbf{M}^{ij\tau s}$	fundamental nucleus of the elemental mass matrix
N	expansion order for TE models
N_i	one-dimensional shape functions
p	polynomial order of the shape functions
$\mathbf{P}$	applied point load
P_x, P_y, P_z	three-dimensional loading components
$\boldsymbol{P}_{\text{ine}}^{i\tau}$	fundamental nucleus of the load due to acceleration fields
$\mathbf{q}$	vector of the nodal generalized displacements
r, s	natural coordinates
r_τ, s_τ	natural coordinates of the Lagrange points
$\mathbf{u}$	three-dimensional displacements vector
$\mathbf{u}_\tau$	generalized displacements vector

u_x, u_y, u_z	three-dimensional displacement components
u_{x1}, u_{y1}, u_{z1},u_{x2}, ..., u_{zM}	generalized displacement components
$\ddot{\mathbf{u}}_0$	applied three-dimensional acceleration field
$\ddot{u}_{x_0}$, $\ddot{u}_{y_0}$, $\ddot{u}_{z_0}$	components of the applied acceleration field
V	beam volume ($V = \Omega \times L$)
$(x,\ y,\ z)$	coordinates reference system
$(x_p,\ y_p,\ z_p)$	application point of the concentrated load
$(x_m,\ y_m,\ z_m)$	application point of the non-structural mass
δ	virtual variation
$\boldsymbol{\epsilon}$	strain vector
λ	Lame's parameter
ρ	material density
ν	Poisson ratio
$\boldsymbol{\sigma}$	stress vector
Ω	cross-section domain

I. Introduction

In engineering practice, problems involving load factors and non-structural masses are of particular interest [1]. A notable example is that of aerospace engineering. In aerospace design, for instance, non-structural masses are used in finite element (FE) models to incorporate the weight of the engines, fuel and payload. On the other hand, the most critical points in the aircraft and spacecraft mission profiles are usually prescribed in terms of load factors. Thus, the importance of having accurate models able to take into account those inertial effects is evident. This aspect is also confirmed by the rich literature on the argument. In [2], for example, structural vibrations of slender missile containing many non-structural masses were carried out by using the method of equivalent density and shell FEs. Ghosh and Ghanem [3] performed random eigenvalue analysis of a Goland wing considering the non-structural masses attached to the wing as a source of uncertainty.

Pagaldipti and Shyy [4] demonstrated the importance of inertial effects on structural analyses and optimal designs. Nikkhoo et al. [5] carried out the vibration analysis of thin rectangular plate due to multiple travelling inertial loads. In the present paper, accurate and efficient one-dimensional (1D) higher-order models able to take into account the effects due to localized inertia and load factors in structural analyses of complex wing structures are proposed and assessed.

Aircraft structures are reinforced thin-shells. These are also called *semimonocoque* constructions, which are obtained by assembling three main components: skins (or panels), longitudinal stiffening members (including spar caps and stringers), and transversal stiffeners (ribs). A brief overview of the evolution and the state-of-the-art of modelling techniques for reinforced-shell structures is given hereafter.

A number of different approaches were developed in the first half of the last century. These are discussed in major reference books [6, 7]. Among these approaches, the so-called *pure semimonocoque* (or "idealized semimonocoque") is the most popular, and it assumes constant shear into panels and webs. The main advantage of this approach is that it leads to a system of linear algebraical equations in the case of static response analysis. However, the number of such equations increases for structures with high redundancies and multi-bay box wings. The number of resulting equations (and redundancies) can be strongly reduced by coupling the pure semimonocoque approach with the assumptions from classical beam theories, such as Euler-Bernoulli Beam Model (EBBM) or Timoshenko Beam Model (TBM).

Due to the advent of computational methods - mostly the Finite Element Method (FEM) - and to the demand for more accuracy, the analysis of complex aircraft structures continued to be made using a combination of solid (3D), plate/shell (2D) and beam (1D) models. The possible manner in which stringers, spar caps, spar webs, panels, and ribs are introduced into FE mathematical models is part of the knowledge of structural analysts and, in general, the coupling of elements with different dimensionality is not trivial. Several works have shown, in fact, the necessity for a proper simulation of the stiffeners-panel "linkage". For example, Satsangi and Murkhopadhyay [8] used 8-node plate elements assuming the same displacement field for stiffeners and plates. Kolli and Chandrashekhara [9] formulated an FE model with 9-node plate and 3-node beam elements. Gangadhara [10] carried

out linear static analyses of composite laminated shells using a combination of 8-node plate elements and 3-node beam elements. With regard to vibration analysis of reinforced-shell structures, which is also one of the topic of the present work, Samanta and Mukhopadhyay [11] developed a new stiffened shell element and, subsequently, they used their formulation to determine natural frequencies and mode shapes of different stiffened structures. Bouabdallah and Batoz [12] presented a finite element model for the static and free vibration analysis of composite cylindrical panels with composite stiffeners. In [13], Thinh and Khoa developed a 9-node stiffened plate element for the modal analysis of laminated stiffened plates with arbitrary oriented stiffeners based on Mindlin's deformation plate theory. Recently, Vörös [14] formulated a new plate/shell stiffener element. In Vörös' theory, the reinforcement is developed employing a general beam theory, including the constraint torsional warping effect and the second order terms of finite rotations.

The works so far mentioned show a definite interest in investigating FEM applications to reinforced-shell structures including inertial effects. However, in most of the articles in literature, such as some of those cited above, plates/shells and stiffeners are modeled separately, and a simulation of the stiffener-panel is often required. Usually, the nodes of the beam elements are connected to those of the shell elements via rigid fictitious links. This technique presents some discrepancies. The principal problems, however, are that the out-of-plane warping displacements in the stiffener section are neglected, and the beam torsional rigidity is not correctly predicted. To overcome those issues, Patel et al. [15] introduced a torsion correction factor. In Vörös' works [14, 16], the connection between the plate/shell and the stiffener was modelled through a special transformation, which included torsional-bending coupling and the eccentricity of internal forces between the stiffener and the plate elements. Conversely, the formulation used in the present paper deals with reinforced-shells using a refined 1D formulation, with no need to introduce "fictitious links" to connect beam and shell elements. This approach is denoted to as *Component-Wise* (CW), and it merely makes use of the physical surfaces of the structures to build a mathematical model. Nowadays, this same result is achievable only by employing 3D solid FE elements.

CW falls within the framework of the Carrera Unified Formulation (CUF), see [17]. CUF is a hierarchical methodology that enables one to develop higher-order theories automatically, without

the need for ad-hoc assumptions. According to CUF, in fact, the displacement field is the expansion of generic functions on the beam cross-section. Depending on the choice of those functions, multiple classes of theories of structures can be formulated. For example, in the case of beam models [18], the Taylor Expansion (TE) class makes use of Taylor-like polynomials to enrich 1D kinematics and it has been validated in various papers in the literature for both static and free vibration analyses (see for example [19]). On the other hand, Lagrange polynomials are used to discretize the displacement field on the cross-section in LE (Lagrange Expansion) CUF beam models, and they are employed in this work to implement CW models of complex wing structures.

In the present paper, CUF is used to formulate and compare various FE beam models - including classical, refined TE and CW ones - of reinforced shell structures. The attention is focused on the capabilities of these beam theories to deal with both static and free vibrations analyses as well as with complex loading conditions due to load factors and non-structural masses, which have been recently introduced and tested in the framework of CUF in [20–22].

The paper is organized as follows: (i) first CUF is introduced and variable kinematic beam theories based on TE are developed; (ii) LE formulation and the related CW approach are then presented; (iii) next, FE arrays, including load vectors due to arbitrary inertial fields, are formulated and expressed in terms of *fundamental nuclei* which do not depend on the theory type and order; (iv) subsequently, various configurations of a benchmark metallic wing are considered and the numerical results are discussed; (v) the main conclusions are finally outlined.

II. Carrera Unified Formulation

A. Classical beam theories and refined kinematics by TE

Figure 1 shows the rectangular cartesian coordinate system and the geometry of the benchmark wing discussed in this work. In the case of simple, preliminary analyses and if sufficiently long, the wing might be modeled by EBBM with acceptable accuracy; the kinematic field of EBBM can be

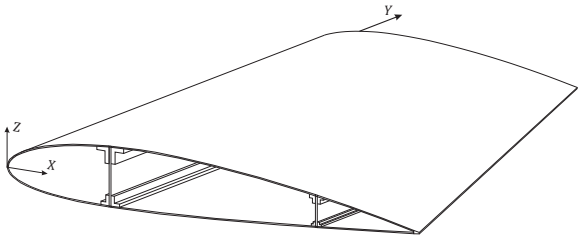

Fig. 1 Coordinate frame of the benchmark aircraft wing

written as

$$\begin{aligned} u_x &= u_{x1} \\ u_y &= u_{y1} - x\,\frac{\partial u_{x1}}{\partial y} + z\,\frac{\partial u_{z1}}{\partial y} \\ u_z &= u_{z1} \end{aligned} \tag{1}$$

where u_x, u_y and u_z are the displacement components of a point belonging to the beam domain along x, y and z, respectively; u_{x1}, u_{y1} and u_{z1} are the displacements of the beam axis; $-\frac{\partial u_{x1}}{\partial y}$ and $\frac{\partial u_{z1}}{\partial y}$ are the rotations of the cross-section about the z- (i.e. ϕ_z) and x-axis (i.e. ϕ_x). According to EBBM, the deformed cross-section remains plane and orthogonal to the beam axis because cross-sectional shear deformation phenomena are neglected. Shear stresses play a significant role in several problems (e.g. short beams, composite structures), and their neglect can lead to incorrect results. One may want to generalize Eq. (1) and overcome the EBBM assumption of the orthogonality of the cross-section. The improved displacement field results in the TBM,

$$\begin{aligned} u_x &= u_{x1} \\ u_y &= u_{y1} + x\,\phi_z + z\,\phi_x \\ u_z &= u_{z1} \end{aligned} \tag{2}$$

TBM constitutes an improvement over EBBM, because the cross-section does not necessarily remain perpendicular to the beam axis after deformation, and two degrees of freedom (i.e. the unknown rotations, ϕ_z and ϕ_x) are added to the original displacement field.

Classical beam models grant reasonably good results when slender, solid section, homogeneous structures undergo bending. On the other hand, the analysis of short, thin-walled, open cross-section beams may require more sophisticated theories to achieve sufficiently accurate results, see [23]. Many refined beam theories have been proposed over the last century to overcome the limitations

of classical beam modelling (e.g. non-fulfillment of homogeneous condition of the transverse stress components at lateral surfaces of the beam); see [19, 24, 25] for a comprehensive review of beam theories. However, as a general guideline, one can state that the richer the kinematic field, the more accurate the 1D model becomes [26]. For example, one can demonstrate that a linear distribution of transverse displacement components (i.e. u_x and u_z) is needed to detect the rigid rotation of the cross-section about the beam axis. Conversely, a third-order displacement field (see [27, 28]) can be adopted to overcome the inconsistency of TBM and fulfill the homogeneous condition of shear stresses on the lateral surfaces. However, richer displacement fields lead to a higher amount of equations to solve and, moreover, the choice of the additional expansion terms is generally problem dependent.

The Carrera Unified Formulation (CUF) can be considered like a tool for tackling the problem of the choice of the expansion terms. Let $\mathbf{u} = \{u_x\, u_y\, u_z\}^T$ be the transposed displacement vector. According to CUF, a generic displacement field can be expressed in a compact fashion as an N-order expansion in terms of generic functions, F_τ,

$$\mathbf{u}(x, y, z) = F_\tau(x, z)\mathbf{u}_\tau(y), \qquad \tau = 1, 2, ..., M \tag{3}$$

where F_τ are the functions of the coordinates x and z on the cross-section; $\mathbf{u}_\tau$ is the vector of the *generalized displacements*; and M stands for the number of terms used in the expansion. Taylor Expansion (TE) CUF models use MacLaurin expansions as F_τ; i.e., 2D polynomials $x^i\, z^j$ (i and j are positive integers) are exploited as basis functions to generate beam theories. It should be noted that Eqs. (1) and (2) are particular cases of the linear ($N = 1$) TE model, which can be expressed as

$$\begin{aligned} u_x &= u_{x_1} + x\, u_{x_2} + z\, u_{x_3} \\ u_y &= u_{y_1} + x\, u_{y_2} + z\, u_{y_3} \\ u_z &= u_{z_1} + x\, u_{z_2} + z\, u_{z_3} \end{aligned} \tag{4}$$

where the parameters on the right-hand side (u_{x_1}, u_{y_1}, u_{z_1}, u_{x_2}, etc.) are the displacements of the beam axis and their first derivatives. Higher-order terms can be taken into account according to Eq. (3). For instance, it is clear that the displacement field of the third-order Reddy's model [28]

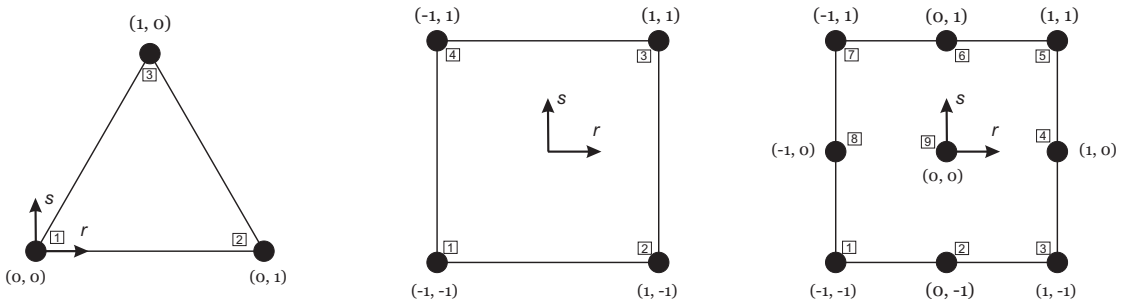

(a) Three-point element, L3 (b) Four-point element, L4 (c) Nine-point element, L9

Fig. 2 Cross-section L-elements in natural geometry

can be considered as a particular case of the $N = 3$ TE model; i.e.

$$\begin{aligned} u_x &= u_{x_1} + x\, u_{x_2} + z\, u_{x_3} + x^2\, u_{x_4} + xz\, u_{x_5} + z^2\, u_{x_6} + x^3\, u_{x_7} + x^2 z\, u_{x_8} + xz^2\, u_{x_9} + z^3\, u_{x_{10}} \\ u_y &= u_{y_1} + x\, u_{y_2} + z\, u_{y_3} + x^2\, u_{y_4} + xz\, u_{y_5} + z^2\, u_{y_6} + x^3\, u_{y_7} + x^2 z\, u_{y_8} + xz^2\, u_{y_9} + z^3\, u_{y_{10}} \\ u_z &= u_{z_1} + x\, u_{z_2} + z\, u_{z_3} + x^2\, u_{z_4} + xz\, u_{z_5} + z^2\, u_{z_6} + x^3\, u_{z_7} + x^2 z\, u_{z_8} + xz^2\, u_{z_9} + z^3\, u_{z_{10}} \end{aligned} \tag{5}$$

The possibility of dealing with arbitrary expansion makes the TE CUF models able to handle complex problems, such as thin-walled structures and local effects.

B. Lagrange Expansion (LE) models and Component-Wise (CW) approach

The degrees of freedom of the TE models described above (i.e., displacements and N-order derivatives of displacements) are defined along the axis of the beam. The unknown variables are only pure displacements if Lagrange polynomials are adopted as expanding functions (F_τ) in Eq. (3). The resulting models are referred to as LE (Lagrange Expansion) and they were first introduced in [29]. Recently, LE beam theory has been utilized for the Component-Wise (CW) modelling of complex structures, namely aerospace [30, 31] and civil engineering [32] structures. The term CW refers to the fact that Lagrange elements are used to model the displacement variables in each structural component at the cross-sectional level.

In this work, three types of cross-sectional Lagrange polynomial sets were adopted to build CW models, and they are shown in Fig. 2. In particular, three-point linear (L3), four-point bi-linear (L4), and nine-point bi-quadratic (L9) polynomials were used. The isoparametric formulation was exploited to deal with arbitrary shaped geometries. The Lagrange polynomials can be found in [33].

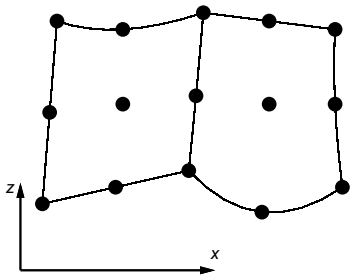

Fig. 3 Two assembled L9 elements in actual geometry

However, the interpolation functions in the case of the L9 element are given as an example

$$F_\tau = \tfrac{1}{4}(\mathsf{r}^2 + \mathsf{r}\,\mathsf{r}_\tau)(\mathsf{s}^2 + \mathsf{s}\,\mathsf{s}_\tau) \qquad \tau = 1,3,5,7$$

$$F_\tau = \tfrac{1}{2}\mathsf{s}_\tau^2(\mathsf{s}^2 - \mathsf{s}\,\mathsf{s}_\tau)(1-\mathsf{r}^2) + \tfrac{1}{2}\mathsf{r}_\tau^2(\mathsf{r}^2 - \mathsf{r}\,\mathsf{r}_\tau)(1-\mathsf{s}^2) \qquad \tau = 2,4,6,8 \tag{6}$$

$$F_\tau = (1-\mathsf{r}^2)(1-\mathsf{s}^2) \qquad \tau = 9$$

where r and s vary from -1 to $+1$, whereas r_τ and s_τ are the coordinates of the nine points whose numbering and location in the natural coordinate frame are summarized in Fig. 2c. The displacement field given by an L9 element is therefore

$$\begin{aligned} u_x &= F_1\, u_{x_1} + F_2\, u_{x_2} + ... + F_9\, u_{x_9} \\ u_y &= F_1\, u_{y_1} + F_2\, u_{y_2} + ... + F_9\, u_{y_9} \\ u_z &= F_1\, u_{z_1} + F_2\, u_{z_2} + ... + F_9\, u_{z_9} \end{aligned} \tag{7}$$

where $u_{x_1}, ..., u_{z_9}$ are the displacement variables of the problem and they represent the translational displacement components of each of the nine points of the L9 element. For further refinements, the cross-section can be discretized by using several L-elements as in Fig. 3, where two assembled L9 elements are shown; this is one of the most important characteristics of the CW approach.

Most of the engineering structures are made of different components, such as spar caps, stringers, longerons, ribs and panels in the case of aerospace constructions. However, these components usually have different geometries and scales. Through the CW approach, one can model each typical part of a structure through the 1D CUF LE formulation. In a finite element framework, this means that different components are modelled by means of the same 1D finite element. An example of CW modelling of a typical wing is shown in Fig. 4. According to CW technique, each component of

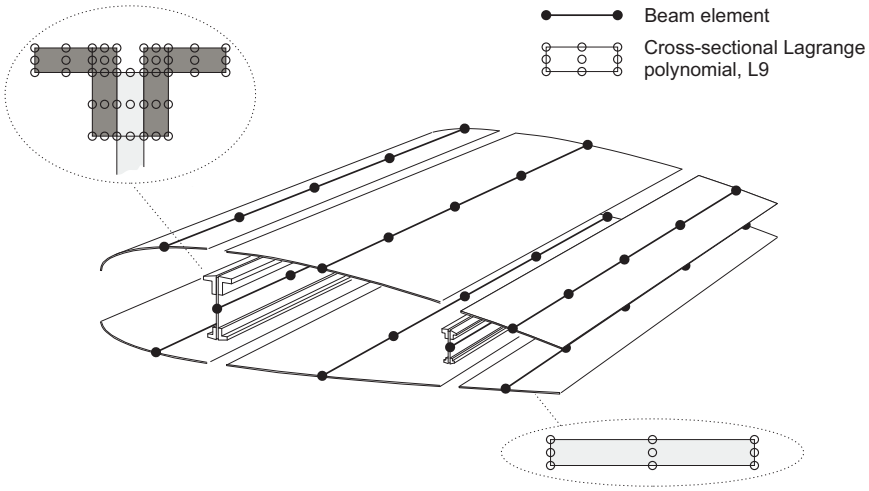

Fig. 4 Component-wise modelling of the benchmark wing

the structure is modelled via beam elements. Then, by exploiting the natural capability of LE to be assembled on the cross-section, Lagrange polynomials (L9 in Fig. 4) are appropriately used to arbitrary refine the beam kinematics. Compatibilities between the various components is enforced in terms of displacements by superimposing cross-sectional nodes. Alternatively, mathematical techniques might be used, see [34, 35]. If a rib were present in the wing in Fig. 4, it would be modelled by beam elements laying on the longitudinal axis, see [30]. One of the main feature of the CW methodology is that it allows for tuning the capabilities of the model by (i) choosing which component requires a more detailed model; and (ii) setting the order of the structural model to be used. Higher-order phenomena (i.e., warping and 3D strain effects) can be, in fact, automatically described by CUF models by opportunely enriching the beam kinematics (see [17, 30]). Moreover, via the CW approach, FE mathematical models can be built by using only physical boundaries; artificial lines (beam axes) and surfaces (plate/shell reference surfaces) are no longer necessary.

III. Finite Element Approximation

A. Fundamental nuclei

The FE approach is adopted to discretize the structure along the y-axis (i.e. the longitudinal axis in Fig. 1). This process is accomplished via a classical finite element technique, where the

displacement vector is given by

$$\mathbf{u}(x,y,z) = F_\tau(x,z)N_i(y)\mathbf{q}_{\tau i}, \qquad \tau = 1,...,M,\ i = 1,...,p+1 \tag{8}$$

N_i stands for the shape functions of order p and $\mathbf{q}_{\tau i}$ is the nodal displacement vector,

$$\mathbf{q}_{\tau i} = \left\{ \begin{array}{ccc} q_{u_{x_{\tau i}}} & q_{u_{y_{\tau i}}} & q_{u_{z_{\tau i}}} \end{array} \right\}^{\mathrm{T}} \tag{9}$$

The shape functions are not given here. They can be found in many books, see for example [36]. Elements with four nodes (B4) were adopted in this work, i.e. a cubic approximation ($p = 3$) along the y axis was assumed. The cross-section discretization for the LE class (i.e., the choice of the type, the number and the distribution of cross-sectional Lagrange elements), or of the theory order N for the TE class, are entirely independent of the choice of the beam finite element to be used along the axis of the beam.

The stiffness and mass matrices, as well as the loading vector of the elements, are obtained via the principle of virtual displacements, which in its general form holds

$$\delta L_{\mathrm{int}} = \int_V \delta\boldsymbol{\epsilon}^{\mathrm{T}}\boldsymbol{\sigma}\,\mathrm{d}V = \delta L_{\mathrm{ext}} - \delta L_{\mathrm{ine}} \tag{10}$$

where L_{int} stands for the strain energy; L_{ext} is the work of the external loads; L_{ine} is the work of the inertial loadings; δ stands for the virtual variation; $V = \Omega \times l$ is the volume of the beam, Ω being the cross-section area are and l the length of the structure; $\boldsymbol{\epsilon}$ and $\boldsymbol{\sigma}$ are the strain and stress vectors, respectively. The virtual variation of the strain energy is rewritten using the constitutive laws, the linear strain-displacement relations, and Eq. (8). It reads

$$\delta L_{\mathrm{int}} = \delta\mathbf{q}_{\tau i}^{\mathrm{T}}\mathbf{K}^{ij\tau s}\mathbf{q}_{sj} \tag{11}$$

where $\mathbf{K}^{ij\tau s}$ is the stiffness matrix in the form of the fundamental nucleus. The derivation of the FE fundamental nucleus of the stiffness matrix is not repeated here for the sake of brevity, but it is given in [17], where more details about CUF can also be found. However, the components of the stiffness matrix nucleus are provided below and they are referred to as $K_{rc}^{ij\tau s}$, where r is the row

number ($r = 1, 2, 3$) and c is the column number ($c = 1, 2, 3$).

$$
\begin{aligned}
K_{11}^{ij\tau s} &= (\lambda + 2G) \int_{\Omega} F_{\tau,x} F_{s,x} \mathrm{d}\Omega \int_{l} N_i N_j \mathrm{d}y + G \int_{\Omega} F_{\tau,z} F_{s,z} \mathrm{d}\Omega \int_{l} N_i N_j \mathrm{d}y + \\
&\quad G \int_{\Omega} F_{\tau} F_{s} \mathrm{d}\Omega \int_{l} N_{i,y} N_{j,y} \mathrm{d}y \\
K_{12}^{ij\tau s} &= \lambda \int_{\Omega} F_{\tau,x} F_{s} \mathrm{d}\Omega \int_{l} N_i N_{j,y} \mathrm{d}y + G \int_{\Omega} F_{\tau} F_{s,x} \mathrm{d}\Omega \int_{l} N_{i,y} N_j \mathrm{d}y \\
K_{13}^{ij\tau s} &= \lambda \int_{\Omega} F_{\tau,x} F_{s,z} \mathrm{d}\Omega \int_{l} N_i N_j \mathrm{d}y + G \int_{\Omega} F_{\tau,z} F_{s,x} \mathrm{d}\Omega \int_{l} N_i N_j \mathrm{d}y \\
K_{21}^{ij\tau s} &= \lambda \int_{\Omega} F_{\tau} F_{s,x} \mathrm{d}\Omega \int_{l} N_{i,y} N_j \mathrm{d}y + G \int_{\Omega} F_{\tau,x} F_{s} \mathrm{d}\Omega \int_{l} N_i N_{j,y} \mathrm{d}y \\
K_{22}^{ij\tau s} &= G \int_{\Omega} F_{\tau,z} F_{s,z} \mathrm{d}\Omega \int_{l} N_i N_j \mathrm{d}y + G \int_{\Omega} F_{\tau,x} F_{s,x} \mathrm{d}\Omega \int_{l} N_i N_j \mathrm{d}y + \\
&\quad (\lambda + 2G) \int_{\Omega} F_{\tau} F_{s} \mathrm{d}\Omega \int_{l} N_{i,y} N_{j,y} \mathrm{d}y \\
K_{23}^{ij\tau s} &= \lambda \int_{\Omega} F_{\tau} F_{s,z} \mathrm{d}\Omega \int_{l} N_{i,y} N_j \mathrm{d}y + G \int_{\Omega} F_{\tau,z} F_{s} \mathrm{d}\Omega \int_{l} N_i N_{j,y} \mathrm{d}y \\
K_{31}^{ij\tau s} &= \lambda \int_{\Omega} F_{\tau,z} F_{s,x} \mathrm{d}\Omega \int_{l} N_i N_j \mathrm{d}y + G \int_{\Omega} F_{\tau,x} F_{s,z} \mathrm{d}\Omega \int_{l} N_i N_j \mathrm{d}y \\
K_{32}^{ij\tau s} &= \lambda \int_{\Omega} F_{\tau,z} F_{s} \mathrm{d}\Omega \int_{l} N_i N_{j,y} \mathrm{d}y + G \int_{\Omega} F_{\tau} F_{s,z} \mathrm{d}\Omega \int_{l} N_{i,y} N_j \mathrm{d}y \\
K_{33}^{ij\tau s} &= (\lambda + 2G) \int_{\Omega} F_{\tau,z} F_{s,z} \mathrm{d}\Omega \int_{l} N_i N_j \mathrm{d}y + G \int_{\Omega} F_{\tau,x} F_{s,x} \mathrm{d}\Omega \int_{l} N_i N_j \mathrm{d}y + \\
&\quad G \int_{\Omega} F_{\tau} F_{s} \mathrm{d}\Omega \int_{l} N_{i,y} N_{j,y} \mathrm{d}y
\end{aligned}
\tag{12}
$$

where G and λ are the Lamé's parameters. If Poisson ν and Young E moduli are used, one has $G = \frac{E}{2(1+\nu)}$ and $\lambda = \frac{\nu E}{(1+\nu)(1-2\nu)}$. The fundamental nucleus has to be expanded according to the summation indexes τ and s in order to obtain the elemental stiffness matrix.

The virtual variation of the work of the inertial loadings is

$$
\delta L_{\mathrm{ine}} = \int_{V} \rho \delta \mathbf{u}^{\mathrm{T}} \ddot{\mathbf{u}} \, \mathrm{d}V \tag{13}
$$

where ρ stands for the density of the material, and $\ddot{\mathbf{u}}$ is the acceleration vector. Equation (13) is

rewritten using Eq. (8)

$$\delta L_{\text{ine}} = \delta \mathbf{q}_{\tau i}^{\mathrm{T}} \int_l N_i N_j \mathrm{d}y \int_\Omega \rho F_\tau F_s \mathrm{d}\Omega \, \ddot{\mathbf{q}}_{sj} = \delta \mathbf{q}_{\tau i}^{\mathrm{T}} \mathbf{M}^{ij\tau s} \ddot{\mathbf{q}}_{sj} \tag{14}$$

where $\mathbf{M}^{ij\tau s}$ is the fundamental nucleus of the mass matrix. Its components are provided below and they are referred to as $M_{rc}^{ij\tau s}$, where r is the row number ($r = 1, 2, 3$) and c denotes column number ($c = 1, 2, 3$).

$$\begin{gathered} \mathbf{M}_{11}^{ij\tau s} = \mathbf{M}_{22}^{ij\tau s} = \mathbf{M}_{33}^{ij\tau s} = \rho \int_l N_i N_j \mathrm{d}y \int_\Omega F_\tau F_s \mathrm{d}\Omega \\ \mathbf{M}_{12}^{ij\tau s} = \mathbf{M}_{13}^{ij\tau s} = \mathbf{M}_{21}^{ij\tau s} = \mathbf{M}_{23}^{ij\tau s} = \mathbf{M}_{31}^{ij\tau s} = \mathbf{M}_{32}^{ij\tau s} = 0 \end{gathered} \tag{15}$$

It is noteworthy that no assumptions about the approximation order have been made in formulating $\mathbf{K}^{ij\tau s}$ and $\mathbf{M}^{ij\tau s}$. It is, therefore, possible to obtain refined beam models without changing the formal expression of the nuclei components. This property of the nuclei is the key-point of CUF that allows, with only nine coding statements, the implementation of any-order of multiple class theories.

The loadings vector which is variationally coherent to the model can be derived with relative ease in the case of a generic concentrated load $\mathbf{P}$ acting on the application point (x_p, y_p, z_p),

$$\mathbf{P} = \left\{ \begin{array}{ccc} P_x & P_y & P_z \end{array} \right\}^T \tag{16}$$

Any other loading condition can be treated similarly. The virtual work due to $\mathbf{P}$ is

$$\delta L_{\text{ext}} = \delta \mathbf{u}^T \mathbf{P} \tag{17}$$

After using Eq. (8), Eq. (17) becomes

$$\delta L_{\text{ext}} = F_\tau N_i \delta \mathbf{q}_{\tau i}^T \mathbf{P} \tag{18}$$

where F_τ and N_i are evaluated in (x_p, z_p) and y_p respectively. The last equation allows the identification of the components of the nucleus that have to be loaded, that is, it allows the proper assembling of the loading vector by detecting the displacement variables that have to be loaded. In the next section, the attention is focused on the special cases of load factors and non-structural masses.

B. Load factors and non-structural masses in the framework of CUF theories

When using classical beam theories, translational as well as rotational load factors are usually applied with respect to the reference axis - or with respect to the shear axis if transverse stresses are also modelled. In this paper, the capability of the present refined beam models to take into account the effects due to 3D distributions of applied inertial loads is also highlighted. Let the following acceleration field be applied to the structure:

$$\ddot{\mathbf{u}}_0(x,y,z) = \left\{ \begin{array}{ccc} \ddot{u}_{x_0} & \ddot{u}_{y_0} & \ddot{u}_{z_0} \end{array} \right\}^T \tag{19}$$

The virtual variation of the external work, δL_{ext}, due to the acceleration field $\ddot{\mathbf{u}}_0$ is given by

$$\delta L_{\text{ext}} = \int_V \rho \delta \mathbf{u}^T \ddot{\mathbf{u}}_0 dV \tag{20}$$

Equation (8) is substituted into Eq. (20). It reads

$$\delta L_{\text{ext}} = \delta \mathbf{q}_{\tau i}^T \Big[\int_\Omega \rho F_\tau F_s \Big(\int_y N_i N_j dy \Big) d\Omega \Big] \ddot{\mathbf{q}}_{sj_0} \tag{21}$$

where the term between square brackets is the fundamental nucleus of the mass matrix $\boldsymbol{M}^{ij\tau s}$. The virtual variation of the external work is, therefore, written as

$$\delta L_{\text{ext}} = \delta \mathbf{q}_{\tau i}^T \, \boldsymbol{M}^{ij\tau s} \, \ddot{\mathbf{q}}_{sj_0} = \delta \mathbf{q}_{\tau i}^T \boldsymbol{P}_{\text{ine}}^{i\tau} \tag{22}$$

where $\boldsymbol{P}_{\text{ine}}^{i\tau}$ is the nucleus of the loading vector due to the acceleration field. It is important to underline that arbitrarily 3D distributed accelerations can be applied for both TE and LE, even though they are beam models.

In the present paper, the effect due to non-structural masses is also investigated. Localized inertia can, in principle, be arbitrarily placed in the 3D domain of the beam structure. In the framework of the CUF, this is easily realized by adding the following term to the fundamental nucleus of the mass matrix:

$$\mathbf{m}^{ijts} = \mathbf{I} \left[F_\tau(x_m, z_m) F_s(x_m, z_m) \, N_i(y_m) N_j(y_m) \right] \tilde{m} \tag{23}$$

where $\mathbf{I}$ is the 3×3 identity matrix and $\tilde{m}$ is the value of the non-structural mass, which is applied at point (x_m, y_m, z_m).

IV. Numerical Results

The present refined 1D models have been evaluated by analyzing several configurations of a metallic benchmark wing, which is depicted in Fig. 1. The considered wing is straight with a NACA 2415 airfoil. The chord c is equal to 1 m. The thickness of each panel is 3 mm, whereas the thickness of the spar webs is 5 mm. The cross-sectional dimensions of the spars caps can be found in [31], together with further details on the benchmark wing. The overall length of the structure is $l = 6$ m. For illustrative purposes, the wing is completely metallic and the adopted material is an aluminium alloy with the following characteristics: elastic modulus $E = 75$ GPa; Poisson ratio $\nu = 0.33$; and density $\rho = 2700$ kg/m^3.

First, the wing configuration with no ribs is assessed. Next, more complex wing structures are discussed to highlight the capabilities of the present beam models to dealing with transverse stiffening members and windows. Both TE and CW models of the benchmark wing were developed, and the correspondent results were compared both with classical beam theories and FE models from the commercial codes MSC Nastran and Abaqus. Regarding those FEM models used for comparisons, both full 3D models and models obtained by combining 2D shell ad 1D beam elements have been considered. Although, the 3D elasticity models have been mainly used for comparing static analyses results because of their capabilities to detect complex strain/stress fields. The solid FEM models were obtained by using eight-node CHEXA Nastran elements. On the other hand, the shell/beam model was obtained by using S4R shell elements for the panels and spars webs and B31 beam elements for the spars caps. The sizes of the finite elements for both the Nastran and Abaqus FE models derived from convergence analyses. Similarly, 8 B4 and 9 B4 elements were respectively used along the beam axis in the case of CW and TE models, which ensured convergent results. In the case of the ribbed configuration, one B4 element for each rib was added.

In the analyses discussed in the following sections, the attention is particularly focussed on the enhanced capability of the present CW models to efficiently deal with complex reinforced structures undergoing inertial loadings, including load factors and localized non-structural masses, both in the case of static response and vibration analyses.

Table 1 Considered load cases

	Point load, F_z		Load factor, n_z	Localized inertia	
	Magnitude (N)	Position	Magnitude (g)	Magnitude (kg)	Position
Load case 1	-3000	④, $y = \frac{2}{3}l$	–	–	–
Load case 2	–	–	1	–	–
Load case 3	–	–	1	300	④, $y = \frac{1}{3}l$

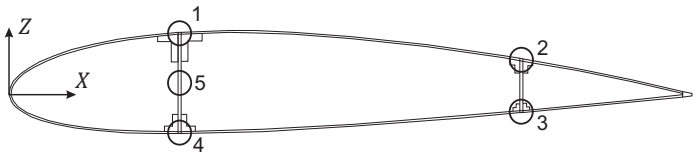

Fig. 5 Notable points on the wing cross-section

A. Static response analyses

Static analysis of the rib-free configuration of the wings is discussed first. Various load cases are considered, and they are summarized in Table 1. The first load case consists of a point load $F_z = -3000$ N placed at point ④ (see Fig. 5) at $y = \frac{2}{3}l$. For the load case under consideration, columns 3 to 5 of Table 2 quote the vertical displacement u_z measured at point ② on the cross-section at the free edge, and the stress components σ_{yy} and σ_{yz} respectively at point ③ on the clamped end and at point ⑤ on the mid-span cross-section. The results from the present higher-order beam formulations based on both TE and LE are shown in Table 2 and compared to the 3D solid model by MSC Nastran. Solutions from classical theories (EBBM and TBM) are also given, and they are retrieved as particular cases of the linear ($N = 1$) TE model. Regarding refined TE models, second- ($N = 2$) to eighth-order ($N = 8$) approximations are quoted in the table. The CW model used for the proposed analysis was built by using a combination of L9 elements on the wing cross-section as outlined in [31]. The number of the degrees of freedom (DOFs) is also given in Table 2 for each model implemented. Figure 6 shows the tip cross-section deformation of the wing by different models for the load case under consideration. Furthermore, Fig. 7 shows the distributions of the shear stress component σ_{yz} by TBM, higher-order TE model, CW, and the MSC Nastran solid solutions. In particular, Fig. 7a shows the trend of the transverse stress through the spanwise direction (y-axis) in correspondence of point ⑤ (see Fig. 5). Moreover, the distribution of σ_{yz} along

Table 2 Selected values of u_z, σ_{yy} and σ_{yz} for various load cases; Wing with no ribs

Models	DOFs	Load case 1			Load case 2			Load case 3		
		$u_z^a\ (mm)$	$\sigma_{yy}^b\ (MPa)$	$\sigma_{yz}^c\ (MPa)$	$u_z^a\ (mm)$	$\sigma_{yy}^b\ (MPa)$	$\sigma_{yz}^c\ (MPa)$	$u_z^a\ (mm)$	$\sigma_{yy}^b\ (MPa)$	$\sigma_{yz}^c\ (MPa)$
Classical models										
EBBM	84	-57.519	-6.648	–	21.572	2.574	–	37.666	5.835	–
TBM	140	-57.563	-6.647	-0.314	21.590	2.574	0.074	37.705	5.835	0.081
Higher-order models based on TE										
$N=2$	504	-55.664	-6.988	-0.339	20.982	2.916	0.058	36.561	7.382	0.064
$N=4$	1260	-56.401	-4.705	-2.099	21.273	2.066	0.525	37.176	5.571	0.551
$N=5$	1764	-56.553	-5.308	-2.391	21.355	2.304	0.574	37.416	6.194	0.670
$N=6$	2352	-56.610	-5.754	-2.470	21.386	2.524	0.595	37.494	6.869	0.760
$N=7$	3024	-56.707	-6.881	-2.848	21.429	2.988	0.726	37.592	7.994	0.898
$N=8$	3780	-56.731	-6.807	-2.908	21.443	2.908	0.739	37.628	7.580	0.903
Higher-order model based on LE										
CW	22200	-56.462	-16.999	-3.182	21.620	7.932	0.638	37.272	15.360	0.317
MSC Nastran model										
Solid	186921	-56.671	-14.185	-3.355	21.818	8.153	0.614	37.657	15.461	0.222

$^a u_z$ at ②, $y=l$; $^b\sigma_{yy}$ at ③, $y=0$; $^c\sigma_{yz}$ at ⑤, $y=l/2$

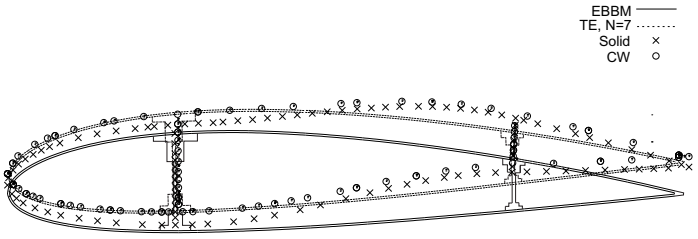

Fig. 6 Tip cross-section deformation under load case 1; Wing with no ribs

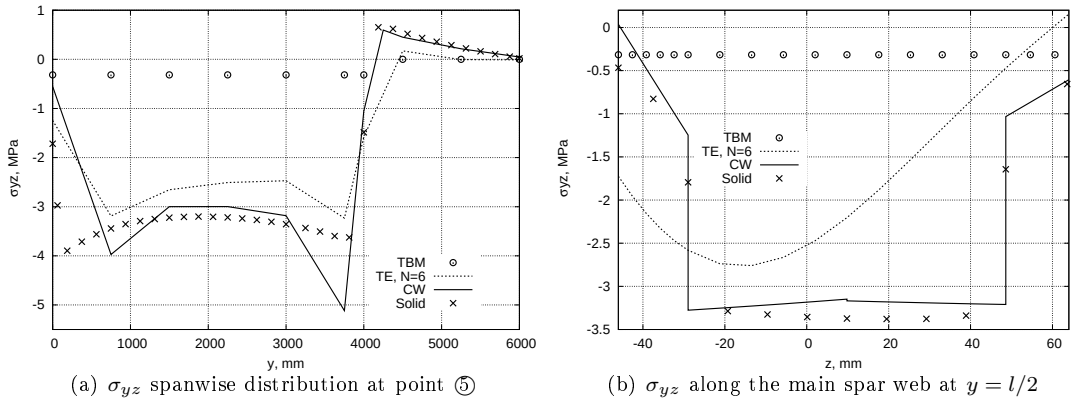

(a) σ_{yz} spanwise distribution at point ⑤ (b) σ_{yz} along the main spar web at $y=l/2$

Fig. 7 Shear stress trends under load case 1; Wing with no ribs

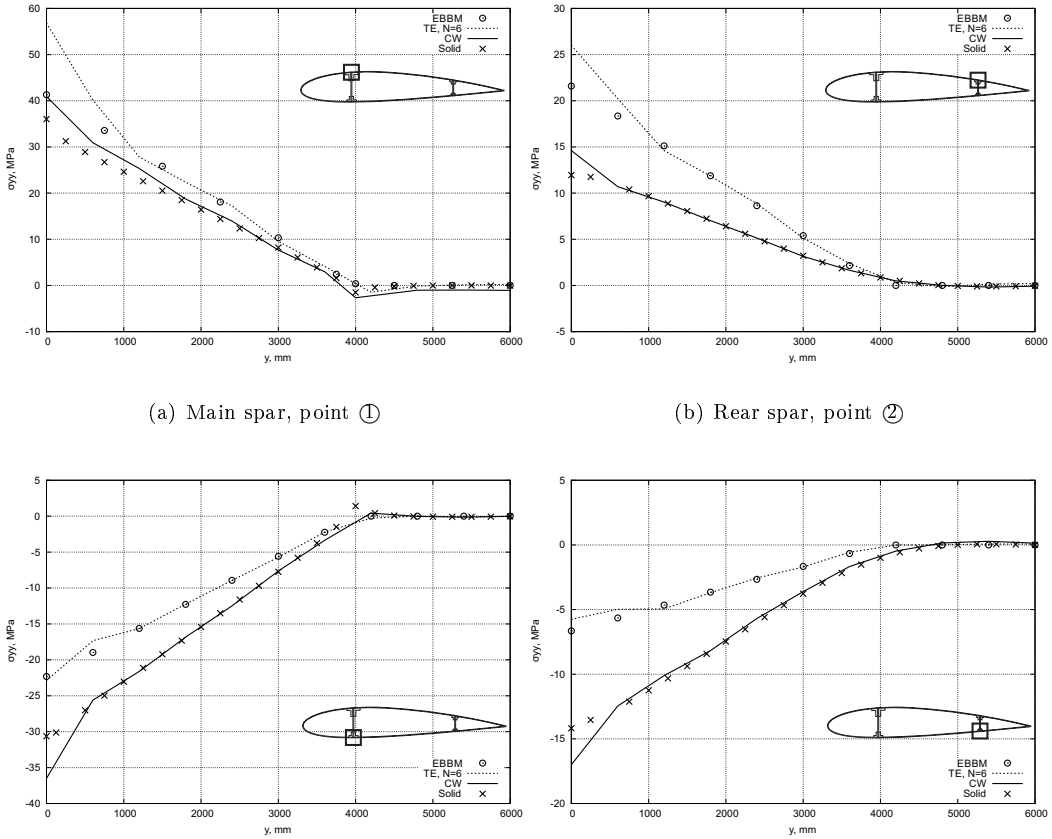

(a) Main spar, point ①

(b) Rear spar, point ②

(c) Main spar, point ④

(d) Rear spar, point ③

Fig. 8 Spanwise axial stress trends under load case 1; Wing with no ribs

the main spar at the mid-span cross-section is depicted in Fig. 7b. Finally, Figure 8 shows the spanwise distribution of the axial stress component σ_{yy} measured at the four spar caps.

In a second load case (see Table 1) the wing underwent an uniform load factor directed to the positive direction of the z-axis. The magnitude of the acceleration field was equal to 1 g, with g being the gravity acceleration. Results in terms of displacements and stress components, which are measured at the same points as in the previous load case, are given in columns 6 to 8 in Table 2. Figure 9 shows the deformation of the tip cross-section by EBBM, the seventh-order ($N = 7$) TE model, the CW model and the MSC Nastran 3D model. It is clear that, even for load case 2, the wing with no rib is still subjected to differential bending deformation.

To further underline the 3D capabilities of the present beam formulation, a non-structural mass was applied at point ⑤ at $y = \frac{1}{3}l$ for load case 3 (see Table 1). The weight of the mass was

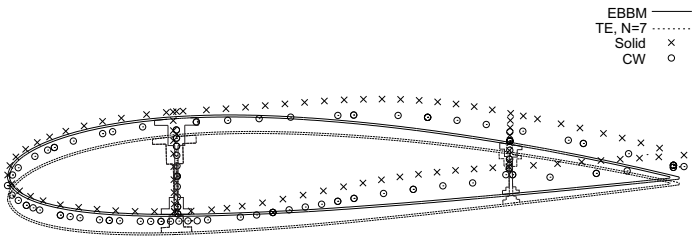

Fig. 9 Tip cross-section deformation under load case 2; Wing with no ribs

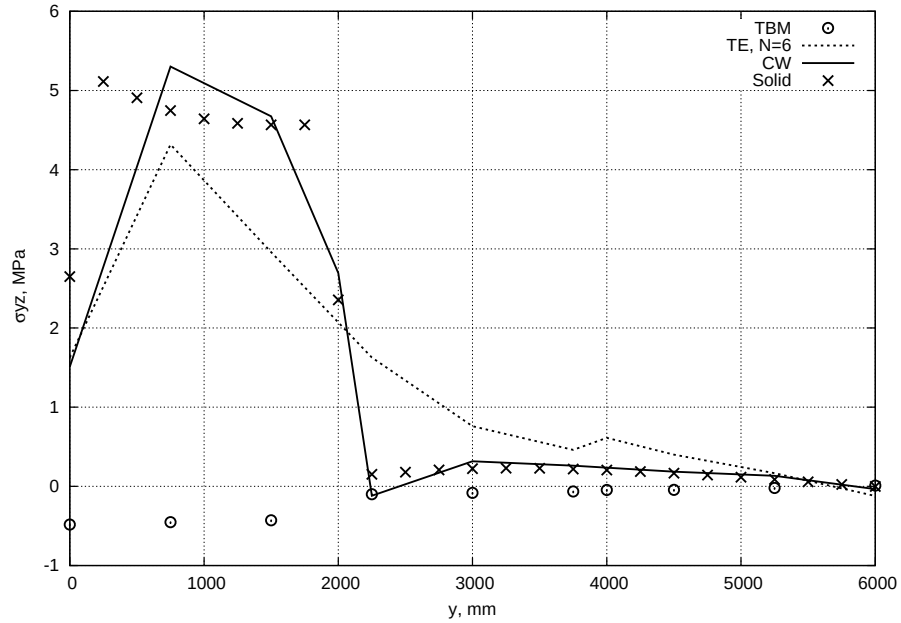

Fig. 10 Spanwise distribution of the transverse shear stress, σ_{yz}, at point ⑤ under load case 3; Wing with no ribs

equal to 300 kg and the same load factor as in load case 2 was enforced. A comparison in terms of displacement and stress components between CW, TE-based and MSC Nastran models is shown in the last columns of Table 2. Finally, Fig. 10 displays the distribution of σ_{yz} along the $y - axis$ for the wing with localized inertia subjected to the unitary load factor. The results of the static analyses of the wing without the ribs underline that

1. Lower- and higher-order models based on TE as well as classical beam models can be locally accurate in terms of displacement and axial stress components (e.g., in the close proximity of the top cap of the main spar). However, those models are not able to correctly describe the overall static response of the wing structure, especially if non-symmetrical loadings are applied and cross-sectional strains/stresses are involved. It is, in fact, clear that, even in the

simple case of axial stress analysis, TE-based CUF models produce some errors that increase close to the clamped section.

2. TE-based models, including EBBM and TBM, are inadequate for detecting transverse shear stress components in spar webs; in particular, TBM underestimates shear because it is not able to foresee torsion and differential bending. In the case of refined TE models the accuracy is slightly increased in terms of shear stresses as the theory order N increases.

3. According to the 3D reference solution, the CW model is perfectly able to foresee the mechanical behaviour of the wing both in terms of displacements and stress field, even if severe differential bending due to non-symmetrical loads (e.g. localized inertia) is involved.

4. The computational efforts demanded by the 1D CW model are significantly lower than those required by the solid Nastran model.

1. Effect of ribs and windows on the static response analysis

Effects due to ribs on the predictive capabilities of the proposed 1D methods for static analysis under inertial loads were also examined. Three ribs with thickness of 6 mm each were, therefore, applied to sections $y = 2$ m, 4 m, and 6 m. Additional details about the modelling of the three-bay wing structure, and in particular the CW modelling of the rib, can be found in [31]. In the proposed analyses, the three-bay wing underwent an uniform load factor, $n_z = 1$ g, directed to the positive verse of z-axis (i.e. load case 2 in Table 1). The results are shown in columns 2 to 5 of Table 3. Both displacement and stress components are given along with the number of DOFs for each model implemented. The measurement points were the same as in the previous analyses. The spanwise distributions of the axial stress components at the spar caps of the three-bay wing are depicted in Fig. 11. On the other hand, Fig. 12 shows the tip cross-section deformation for the case under consideration. The following comments stem from the analysis of the three-bay benchmark wing:

1. Due to ribs, the wing is more rigid within the cross-sectional plane. As a consequence, higher-order effects play a marginal role in this particular wing configuration. For this reason, even classical beam models can be effective in detecting the structure deformation.

Table 3 Selected values of u_z, σ_{yy} and σ_{yz}; Three-bay wing, both without and with underside window, subjected to load case 2

Models	Three-bay wing				Three-bay wing with opening			
	u_z^a (mm)	σ_{yy}^b (MPa)	σ_{yz}^c (MPa)	DOFs	u_z^a (mm)	σ_{yy}^b (MPa)	σ_{yz}^c (MPa)	DOFs
Classical models								
EBBM	22.443	2.677	–	84	22.897	2.532	–	84
TBM	22.440	2.674	0.114	140	22.898	2.551	0.128	140
Higher-order models based on TE								
$N=2$	21.502	3.027	0.087	504	22.004	2.880	0.062	504
$N=4$	21.838	2.414	0.948	1260	22.419	2.275	1.058	1260
$N=5$	21.925	2.591	1.113	1764	22.551	2.449	1.348	1764
$N=6$	21.964	2.887	1.020	2352	22.640	2.733	1.337	2352
$N=7$	22.007	3.135	0.986	3024	22.736	3.020	1.297	3024
$N=8$	22.026	3.121	0.994	3780	22.797	3.011	1.371	3780
Higher-order model based on LE								
CW	22.214	7.873	0.779	24864	23.024	7.658	1.100	24165
MSC Nastran model								
Solid	22.456	7.958	0.726	171321	23.288	6.312	1.033	129183

$^a u_z$ at ②, $y=l$; $^b\sigma_{yy}$ at ③, $y=0$; $^c\sigma_{yz}$ at ⑤, $y=l/2$

2. Stress analysis still requires refined models, although. If compared to the solid model, maximum relative errors close to 70 % for axial stress are still produced by EBBM and TE analyses. However, results in terms of stress components are slightly improved with respect to the analysis of the rib-free configuration.

3. CW models are very effective and efficient, even in the case of wing structures with ribs.

Interesting guidelines for the development of advanced beam models including inertial effects can be extrapolated from the analysis of the ribbed three-bay wing box with an underside window in the mid-bay, which is discussed hereinafter. The cross-section of the mid-bay is shown Fig. 13 in

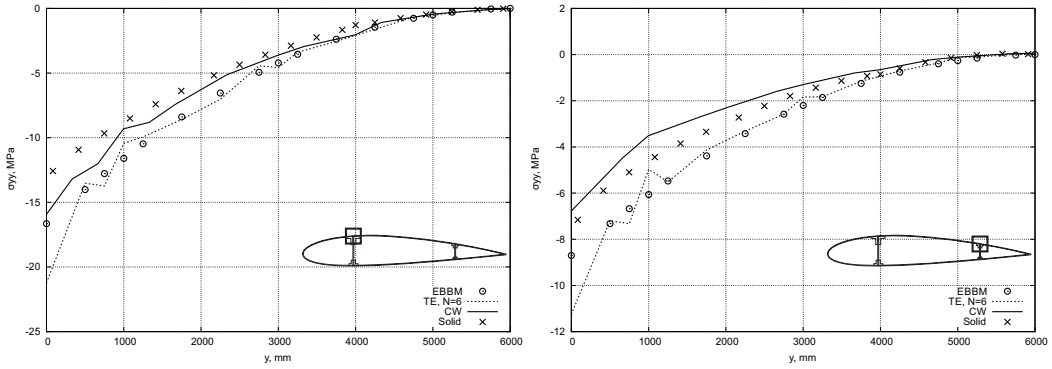

(a) Main spar, point ①

(b) Rear spar, point ②

(c) Main spar, point ④

(d) Rear spar, point ③

Fig. 11 Spanwise axial stress trends under load case 2; Three-bay wing with ribs

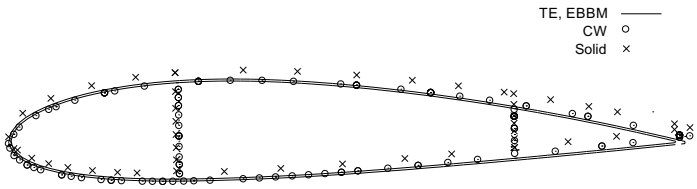

Fig. 12 Tip cross-section deformation under load case 2; Three-bay wing with ribs

order to better highlight the considered geometry. The structure underwent load case 2 as detailed in Table 1. Results in terms of displacements and stress components are reported in the last columns of Table 3. Figure 14 shows the distribution of the axial stress σ_{yy} along the four stringers evaluated according to different models. Finally, for the same load case, Fig. 15 summarizes the comparison of the results in terms of shear stress σ_{yz} between the CW and the Nastran 3D models. In particular, the figure shows the spanwise distribution of the shear stress at the centre of the main spar web for the wing without ribs, the ribbed wing and the ribbed wing with the underside opening at the

Fig. 13 Cross-section of the open mid-bay of the ribbed wing

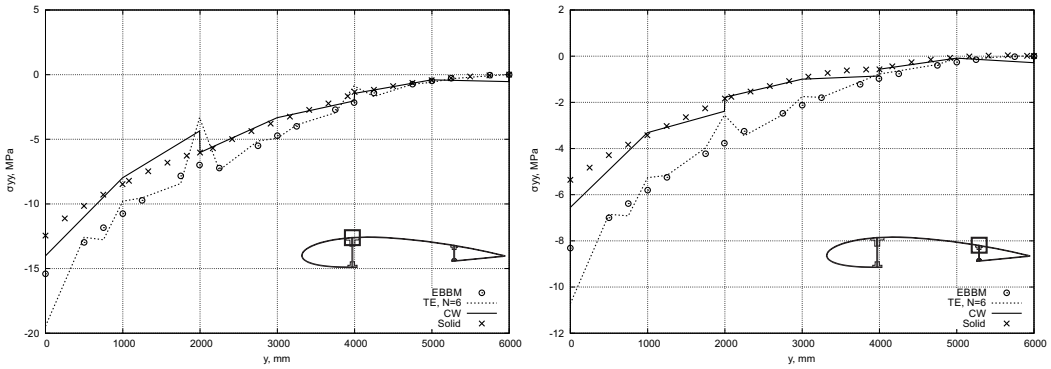

(a) Main spar, point ①

(b) Rear spar, point ②

(c) Main spar, point ④

(d) Rear spar, point ③

Fig. 14 Distribution of axial stress σ_{yy} along the stringers; Three-bay wing with underside window subjected to load case 2

mid-bay. Some further remarks can be made:

1. The window results in concentrations of axial stress in the lower spars caps that are close to the middle bay. This phenomenon is correctly predicted by both CW and Nastran solid model.

2. The shear stress in the spar webs increase as a consequence of the window. Even in this case, the 1D CW model is the best compromise between accuracy and computational efficiency.

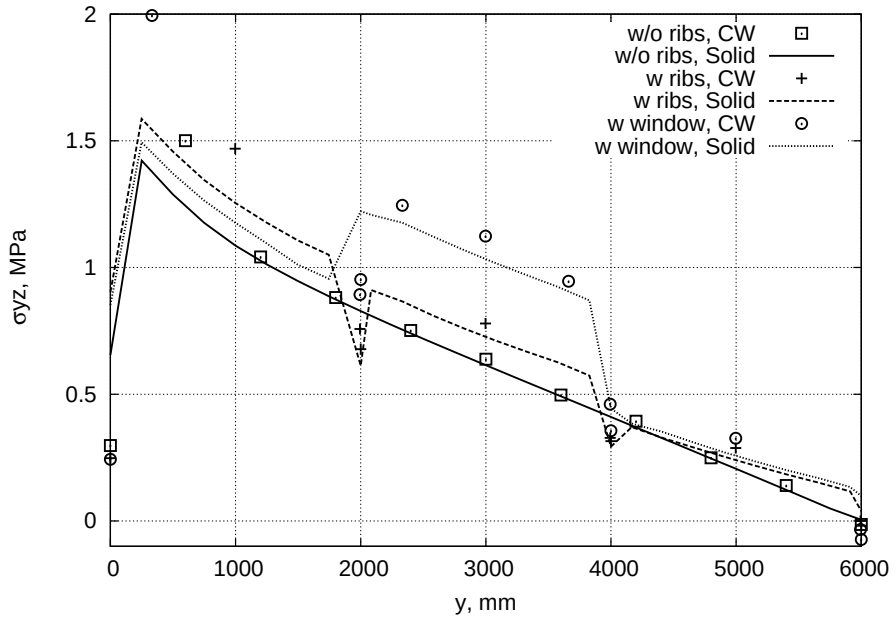

Fig. 15 Comparison of the shear stress σ_{yz} at point ⑤ along the spanwise direction; Various configuration of the benchmark wing undergoing load case 2

3. Classical and TE (even higher-order) models are not recommended for the static analysis of wing structures, especially if windows are present or accurate stress analyses are required.

B. Free vibration analyses

The free vibration characteristics of the metallic benchmark wing are discussed in this section. The configuration with no ribs is addressed first. Table 4 shows the first eight natural frequencies of the wing both without and with a non-structural mass applied. The weight of the non-structural mass was equal to 300 kg and it was applied as in load case 3 (see Table 1). In Table 4, the results by the classical beam models (EBBM and TBM) are given in columns 2 and 3. The natural frequencies according to the the second- ($N = 2$), fourth- ($N = 4$), sixth- ($N = 6$) and eighth-order (N=8) refined TE beam models are given in columns 4 to 7. The results of the CW model are quoted in column 8. In the last column of Table 4, the MSC Nastran solid solution is given for comparison purposes. The number of DOFs is also given in the table for comparing the computational demand for each model. As it is clear, bending, torsional, coupled bending-torsional, and *shell-like* modes were detected in the proposed analysis. A shell-like mode is a modal shape that involves cross-section deformation. The term “shell" is used because this kind of mode is usually foreseen by 2D

Table 4 First 8 natural frequencies (Hz)

Mode	Natural Frequencies (Hz)							
	Classical and refined models based on TE						LE model	Nastran model
	EBBM	TMB	$N=2$	$N=4$	$N=6$	$N=8$	CW	Solid
Bending[a]	4.22	4.22	4.29	4.26	4.25	4.24	4.23	4.21
Bending[b]	22.08	21.81	21.94	21.85	21.80	21.75	21.75	21.68
Bending[a]	26.46	26.37	26.69	26.19	26.05	25.92	25.14	24.77
Torsional	-	-	50.34	47.73	43.59	42.43	31.13	29.17
Bending[a]	73.97	73.42	74.08	71.30	70.56	69.55	59.25	56.11
Bending[a]	134.58	124.62	143.34	134.23	131.64	126.76	66.65	62.41
Shell − like	-	-	-	-	-	-	74.22	68.77
Shell − like	-	-	-	-	-	-	88.93	73.85
	Frequencies with non-structural mass							
	Classical and refined models based on TE						LE model	Nastran model
	EBBT	TMB	$N=2$	$N=4$	$N=6$	$N=8$	CW	Solid
Bending[a]	3.82	3.81	3.88	3.84	3.83	3.82	3.82	3.80
Bending[a]	14.17	14.10	13.37	12.87	12.50	12.06	13.34	13.16
Bending[b]	19.85	19.48	19.60	19.46	19.38	19.21	19.31	19.19
Torsional	-	-	42.61	40.78	38.41	37.34	28.79	27.02
Coupled	-	-	57.74	55.12	52.39	44.38	45.10	43.14
Shell − like	-	-	-	-	-	-	51.92	48.96
Shell − like	-	-	-	-	-	-	59.35	56.65
Shell − like	-	-	-	-	-	-	78.20	71.45
DOFs	84	140	504	1260	2352	3780	22200	186921

a: bending within yz-plane; b: bending within xy-plane

plate/shell models. In Fig. 16 the Modal Assurance Criterion (MAC) matrix between the CW and the solid model is shown to further underline the good accuracy of the proposed methodology. MAC is, in fact, defined as a scalar representing the degree of consistency between two distinct modal vectors (see Ref.[37]) as follows:

$$\mathrm{MAC}_{ij} = \frac{|\{\phi_{A_i}\}^T\{\phi_{B_j}\}|^2}{\{\phi_{A_i}\}^T\{\phi_{A_i}\}\{\phi_{B_j}\}\{\phi_{B_j}\}^T} \tag{24}$$

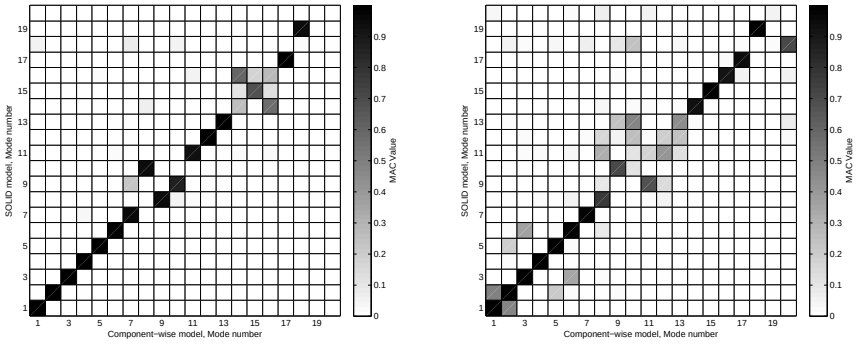

(a) Without non-structural mass (b) With non-structural mass

Fig. 16 MAC values between CW and MSC Nastran solid models for wing with no ribs

where $\{\phi_{A_i}\}$ is the i^{th} eigenvector of model A, whereas $\{\phi_{B_j}\}$ is the j^{th} eigenvector of model B. The modal assurance criterion takes on values from zero (representing no consistent correspondence), to one (representing a consistent correspondence). Both the case with and without localized inertia is shown in Fig. 16. Finally, some selected modal shapes of the CW model compared with the MSC Nastran solution are shown in Fig. 17. The free vibration analyses of the rib-free configuration highlight that

1. Classical, higher-order TE and CW models are able to detect the first bending modes.

2. Because of differential bending phenomena, which are further magnified by the non-structural mass, higher bending frequencies are not correctly represented by classical and refined TE beam models; CW or 3D elasticity models are needed instead.

3. At least a second-order ($N = 2$) TE model is needed to detect torsional modes. However, very high order of expansion are necessary in the case of TE to correctly catch the related natural frequencies.

4. TE models are not able to detect shell-like frequencies. Those modes are instead correctly identified by the CW models, which are in good agreement with the Nastran models.

5. CW model replicates the solution obtained by MSC Nastran both in terms of frequencies and modal shapes. The mean error between the two models calculated according to the first eight frequencies, in fact, is about 6%; it decrease to 4% in case of non-structural mass. Moreover,

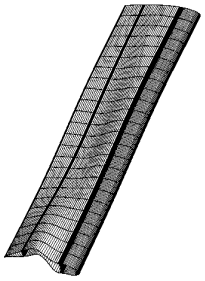

(a) Mode 6, CW model (66.65 Hz)

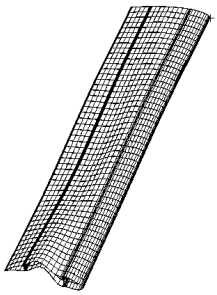

(b) Mode 6, Solid model (62.41 Hz)

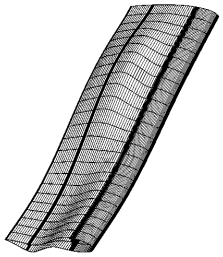

(c) Mode 7 with non-structural mass, CW model (59.35 Hz)

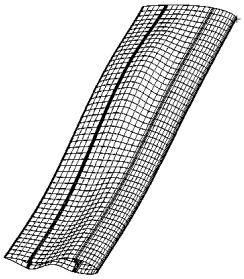

(d) Mode 7 with non-structural mass, Solid model (56.65 Hz)

Fig. 17 Selected modal shapes for wing with no ribs

according to the MAC analyses, the first 19 modes are correctly described by the CW model, even though those modes not always occupy the same positions in the eigenvectors matrix with respect to the solid model. For example, modes 9 to 13 are slightly different between CW and Nastran model if a non-structural mass is applied because coupling phenomena occur.

1. Free vibrations of the three-bay configuration

The effects of the ribs on the free vibrations of the considered wing structure are further investigated, and the efficiency of the proposed 1D models verified. Table 5 shows the first eight natural frequencies from the various models examined. The frequencies of the wing with non-structural mass as in the previous analysis are also given in Table 5. In the study case with no localized inertia, the results by a Shell/Beam Abaqus model are also presented together with the results from the other models discussed so far. The correspondence between the modal shapes obtained by the

Table 5 First 8 natural frequencies (Hz), wing with ribs.

Mode	Natural Frequencies (Hz)								
	Classical and refined models based on TE						LE model	Nastran and Abaqus models	
	EBBM	TMB	$N=2$	$N=4$	$N=6$	$N=8$	CW	Solid	Shell/Beam
Bending[a]	4.12	4.12	4.18	4.14	4.15	4.15	4.14	4.12	4.43
Bending[b]	21.55	21.28	21.38	21.28	21.33	21.28	21.30	21.22	21.58
Bending[a]	25.73	25.65	25.92	25.43	25.41	25.30	25.07	24.92	26.32
Torsional	-	-	49.69	47.07	43.10	42.18	39.53	39.22	36.89
Bending[a]	71.50	70.96	71.56	68.90	68.53	67.90	65.29	63.87	63.40
Shell − like	-	-	-	-	-	-	85.85	75.01	67.73
Shell − like	-	-	-	-	-	-	91.70	78.60	70.49
Shell − like	-	-	-	-	-	-	93.65	80.43	72.74
	Frequencies with non-structural mass								
	Classical and refined models based on TE						LE model	Nastran model	
	EBBT	TMB	$N=2$	$N=4$	$N=6$	$N=8$	CW	Solid	
Bending[a]	3.74	3.74	3.82	3.79	3.78	3.77	3.76	3.74	
Bending[a]	13.98	13.91	14.15	13.84	13.74	13.67	13.56	13.51	
Bending[b]	19.54	19.17	19.36	19.23	19.16	19.09	19.05	18.96	
Torsional	-	-	44.03	41.88	38.95	38.20	35.66	35.38	
Bending[a]	51.83	51.49	55.31	53.41	52.41	51.95	50.47	50.13	
Coupled	-	-	65.44	63.35	61.73	60.59	59.18	58.73	
Shell − like	-	-	-	-	-	-	83.27	74.55	
Shell − like	-	-	-	-	-	-	87.65	76.38	
DOF	84	140	504	1260	2352	3780	24864	171321	119712

a: bending within yz plane; b: bending within xy plane

MSC Nastran 3D solid and the CW models was further investigated through MAC analyses, which are shown in Fig. 18. Some selected modal shapes are finally depicted in Fig. 19. The following statements hold:

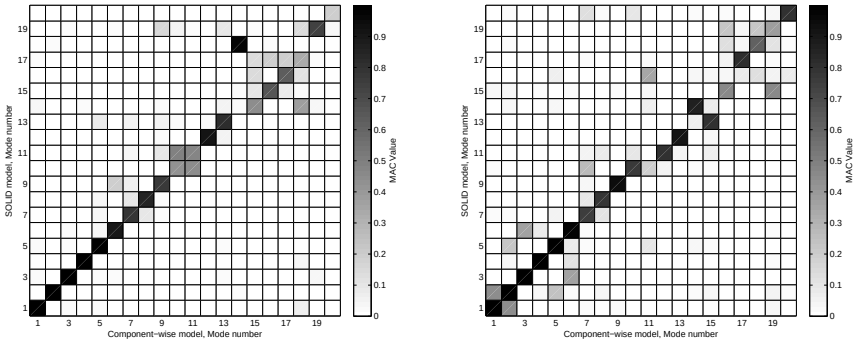

(a) Without non-structural mass (b) With non-structural mass

Fig. 18 MAC values between CW and MSC Nastran solid model for wing with ribs

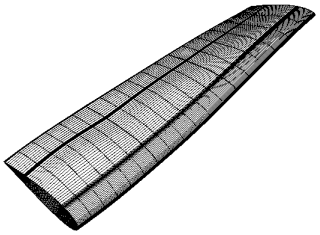

(a) Mode 4, CW model (39.53 Hz)

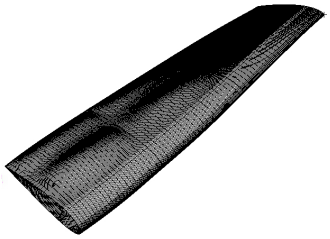

(b) Mode 4, Solid model (39.22 Hz)

(c) Mode 5 with non-structural mass, CW model (50.47 Hz)

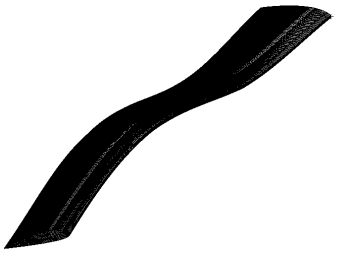

(d) Mode 5 with non-structural mass, solid model (50.13 Hz)

Fig. 19 Selected modal shapes for wing with ribs

1. The overall accuracy of the proposed beam models is globally improved because of the ribs. Those transversal stiffening members, in fact, limit the cross-sectional deformation in accordance with classical beam modelling hypotheses. Thus, bending frequencies are correctly described by relatively low-order beams, such the fourth-order ($N = 4$) TE model. Classical

models are still inaccurate for higher bending frequencies.

2. If localized inertia is considered, the related coupled modes need higher-order approximations in the case of TE.

3. The Shell/Beam Abaqus model produces some errors, even at the first bending frequencies. These errors are due to the geometrical inconsistency of the model. In fact, fictitious lines and planes are employed in the Abaqus model in order to define the domains for the 1D and 2D FE approximations. Thus, unlikely the 3D solid and the proposed beam models, a fictitious geometry is used in the Shell/Beam mathematical description. However, these kind of models are widely used in common practice, and their accuracy can be, in principle, improved by exploiting experimental testing and model updating.

4. The CW approach only exploits real physical surfaces to model the structure. That was only possible till now by using solid models.

5. The correspondence between the CW and the Nastran solid model is excellent and improved with respect to the previous analysis where ribs were not considered. As shown by MAC, in fact, even if non-structural masses are employed and coupled phenomena are present, the mode shapes by the CW model match those by the reference solid model.

V. Conclusions

Various finite beam elements able to include spatially distributed load factors and non-structural masses have been formulated and applied to the analysis of metallic wing structures. The proposed models have been formulated by using the Carrera Unified Formulation (CUF), which is a tool for the automatic implementation of variable kinematic theories. The 3D displacement field is, in fact, approximated through arbitrary cross-sectional functions in the framework of 1D CUF. According to previous research, refined beam models are formulated by making use of either Taylor-like or Lagrange cross-sectional approximations. The former class of polynomials results in TE (Taylor Expansion) models. Classical beam theories are particular cases of the TE linear model. If Lagrange polynomials are employed on the beam cross-section, the resulting elements have only pure

displacement variables, and they have been referred to as LE (Lagrange Expansion). By exploiting the natural capabilities of LE models to be assembled at the cross-sectional level, the Component-Wise (CW) approach has been formulated and discussed in this paper. CW is very efficient for the analysis of multi-component structures, such as aerospace ones, because it allows the analysts to use only the physical surfaces in the development of the mathematical model. Moreover, each component of the structure (e.g. spars, ribs, panels, etc.) is modelled by the same finite element in the framework of CW.

In this work, particular attention has been focussed on static and free vibration analysis of wing structures subjected to external inertial loads, such as load factors and non-structural masses. The capabilities of the proposed beams have been investigated for various wing configurations, including ribbed wings, and the effects due to underside windows have been evaluated. The results have been compared to solutions from commercial FEM tools. In particular, both solid and shell/beam FE models have been considered. The analyses highlight the following concluding remarks:

1. Classical beam theories cannot, of course, deal with arbitrarily distributed load factors and localized inertiae. Moreover, those beam models are effective only if deformation response of multi-bay wings under bending are considered.

2. Higher-order TE models may be affected by severe errors in stress analyses, even if symmetric loading conditions and simple wing configurations are analysed.

3. FE models built by assembling 2D/shell and 1D/beam elements can be affected by inconsistencies due to geometrical approximations demanded by modelling techniques.

4. CW models only use physical surfaces in modelling wing structures, and they are the best compromise in terms of accuracy and efficiency if: (i) accurate stress analysis is required; (ii) non-negligible cross-sectional deformations, e.g. due to differential bending, are involved; (iii) geometrical discontinuities, such as windows, are present; (iv) coupling phenomena due, for example, to complex loadings, including load factors and non-structural masses, are considered; (v) accurate free vibration analysis involving couplings and shell-like mode shapes are needed. CW models have, in fact, been successfully compared to complex 3D FEM models by

MSC Nastran, which presented approximately one order of magnitude of DOFs more.

References

[1] Kamat, M., "Effect of shear deformations and rotary inertia on optimum beam frequencies," *International Journal for Numerical Methods in Engineering*, Vol. 9, No. 1, 1975, pp. 51–63.

[2] Zhang, Q. and Liu, L., "Modal analysis of missile's equivalent density finite element model," *Binggong Xuebao/Acta Armamentarii*, Vol. 29, No. 11, 2008, pp. 1395–1399.

[3] Ghosh, D. and Ghanem, R., "Random eigenvalue analysis of an airframe," in "45th AIAA/ASME/ASCE/AHS/ASC Structures, Structural Dynamics and Materials Conference," American Institute of Aeronautics and Astronautics Inc. (AIAA), Palm Springs, California, 2004.

[4] Shenyan, C., "Structural modeling and design optimization of spacecraft," *Advances in the Astronautical Sciences*, Vol. 117, 2004, pp. 139–145.

[5] Nikkhoo, A., Hassanabadi, M., Azam, S., and Amiri, J., "Vibration of a thin rectangular plate subjected to series of moving inertial loads," *Mechanics Research Communications*, Vol. 55, 2014, pp. 105–113, doi:10.1016/j.mechrescom.2013.10.009.

[6] Bruhn, E. F., *Analysis and Design of Flight Vehicle Structures*, Tri-State Offset Company, 1973.

[7] Rivello, R. M., *Theory and analysis of flight structures*, McGraw-Hill, 1969.

[8] Satsangi, S. and Mukhopadhyay, M., "Finite element state analysis of girder bridges having arbitrary platform," *Int. Ass. of Bridge Struct. Engng.*, Vol. 17, 2006, pp. 65–94.

[9] Kolli, M. and Chandrashekhara, K., "Finite element analysis of stiffened laminated plates under transverse loading," *Composite Science and Technology*, Vol. 56, 1996, pp. 1355–1361.

[10] Gangadhara Prusty, B., "Linear static analysis of hat stiffened laminated shells using finite elements," *Finite elements in analysis and design*, Vol. 39, 2003, pp. 1125–1138.

[11] Samanta, A. and Mukhopadhyay, M., "Free vibration analysis of stiffened shells by the finite element technique," *European Journal of Mechanics - A/Solids*, Vol. 23, No. 1, 2004, pp. 159 – 179. DOI: 10.1016/j.euromechsol.2003.11.001.

[12] Bouabdallah, M. and Batoz, J., "Formulation and evaluation of a finite element model for the linear analysis of stiffened composite cylindrical panels," *Finite Elements in Analysis and Design*, Vol. 21, No. 4, 1996, pp. 265–289. DOI: 10.1016/0168-874X(95)00047-W.

[13] Thinh, T. I. and Khoa, N. N., "Free Vibration Analysis of Stiffened Laminated Plates Using a New Stiffened Element," *Technische Mechanikl*, Vol. 28, 2008, pp. 227–236.

[14] Vörös, G. M., "Finite element analysis of stiffened plates," *Periodica Polytechnica*, Vol. 51, No. 2, 2007,

pp. 105–112. DOI: 10.3311/pp.me.2007-2.10.

[15] Patel, S. N., Datta, P. K., and Seikh, A. H., "Buckling and dynamic instability analysis of stiffened shell panels," *Thin-Walled Structures*, Vol. 44, 2006, pp. 321–333.

[16] Vörös, G. M., "A special purpose element for shell-beam systems," *Computers and Structures*, Vol. 29, No. 2, 1988, pp. 301–308.

[17] Carrera, E., Cinefra, M., Petrolo, M., and Zappino, E., *Finite Element Analysis of Structures through Unified Formulation*, John Wiley & Sons, 2014.

[18] Carrera, E., Giunta, G., and Petrolo, M., *Beam Structures: Classical and Advanced Theories*, John Wiley & Sons, 2011. DOI: 10.1002/9781119978565.

[19] Carrera, E., Pagani, A., Petrolo, M., and Zappino, E., "Recent developments on refined theories for beams with applications," *Mechanical Engineering Reviews*, Vol. 2, No. 2,
doi:10.1299/mer.14-00298.

[20] Carrera, E., Pagani, A., and Zangallo, F., "Thin-walled beams subjected to load factors and non-structural masses," *International Journal of Mechanical Sciences*, Vol. 81, 2014, pp. 109–119,
doi:10.1016/j.ijmecsci.2014.02.015.

[21] Pagani, A., Zangallo, F., and Carrera, E., "Influence of non-structural localized inertia on free vibration response of thin-walled structures by variable kinematic beam formulations," *Shock and Vibration*, Vol. 2014,
doi:10.1155/2014/141982.

[22] Carrera, E., Pagani, A., and Zangallo, F., "Comparison of various 1D, 2D and 3D FE models for the analysis of thin-walled box with transverse ribs subjected to load factors," *Finite Elements in Analysis and Design*, Vol. 95, 2014, pp. 1–11,
doi:10.1016/j.finel.2014.10.004.

[23] Novozhilov, V. V., *Theory of Elasticity*, Pergamon Press, 1961.

[24] Kapania, K. and Raciti, S., "Recent Advances in Analysis of Laminated Beams and Plates, Part I: Shear Effects and Buckling," *AIAA Journal*, Vol. 27, No. 7, 1989, pp. 923–935.

[25] Kapania, K. and Raciti, S., "Recent Advances in Analysis of Laminated Beams and Plates, Part II: Vibrations and Wave propagation," *AIAA Journal*, Vol. 27, No. 7, 1989, pp. 935–946.

[26] Washizu, K., *Variational Methods in Elasticity and Plasticity*, Pergamon, Oxford, 1968.

[27] Vlasov, V. Z., *Thin-walled elastic beams*, National Science Foundation, Washington, 1961.

[28] Heyliger, P. R. and N., R. J., "A higher order beam finite element for bending and vibration problems," *Journal of Sound and Vibration*, Vol. 126, No. 2, 1988, pp. 309–326.

[29] Carrera, E. and Petrolo, M., "Refined Beam Elements with only Displacement Variables and Plate/Shell Capabilities," *Meccanica*, Vol. 47, No. 3, 2012, pp. 537–556. DOI: 10.1007/s11012-011-9466-5.

[30] Carrera, E., Pagani, A., and Petrolo, M., "Classical, Refined and Component-wise Theories for Static Analysis of Reinforced-Shell Wing Structures," *AIAA Journal*, Vol. 51, No. 5, 2013, pp. 1255–1268, doi:10.2514/1.J052331.

[31] Carrera, E., Pagani, A., and Petrolo, M., "Component-wise Method Applied to Vibration of Wing Structures," *Journal of Applied Mechanics*, Vol. 80, No. 4, 2013, p. 041012, doi:10.1115/1.4007849.

[32] Carrera, E., Pagani, A., and Petrolo, M., "Refined 1D Finite Elements for the Analysis of Secondary, Primary, and Complete Civil Engineering Structures," *Journal of Structural Engineering*, p. 04014123, doi:10.1061/(ASCE)ST.1943-541X.0001076.

[33] Oñate, E., *Structural Analysis with the Finite Element Method: Linear Statics, Volume 1*, Springer, 2009.

[34] Carrera, E., Pagani, A., and Petrolo, M., "Use of Lagrange Multipliers to Combine 1D Variable Kinematic Finite Elements," *Computers and Structures*, Vol. 129, 2013, pp. 194–206, doi:10.1016/j.compstruc.2013.07.005.

[35] Carrera, E. and Pagani, A., "Analysis of Reinforced and Thin-walled Structures by Multi-line Refined 1D/Beam Models," *International Journal of Mechanical Sciences*, Vol. 75, 2013, pp. 278–287, doi:10.1016/j.ijmecsci.2013.07.010.

[36] Bathe, K., *Finite element procedure*, Prentice hall, 1996.

[37] Allemang, R. J. and Brown, D. L., "A Correlation Coefficient for Modal Vector Analysis," in "Proceedings of the International Modal Analysis Conference," , 1982, pp. 110–116.